Surface Grating Optimization for Low-Threshold Atomic Clock VCSELs

Md. Jarez Miah, Ahmed Al-Samaneh, and Pierluigi Debernardi

Vertical-cavity surface-emitting lasers (VCSELs) with emission in a single-mode, single-polarization beam at a wavelength of 894.6 nm have been fabricated for use in Cs-based atomic clocks. For polarization control, monolithically integrated surface gratings are employed. Simulated and experimental results show that the longitudinal position of the surface grating has a significant influence on the threshold current. With a grating in the topmost in-phase layer, the threshold currents are reduced to 40 % compared to earlier atomic clock grating VCSELs with inverted structure. The output polarization is parallel to the grating lines with a peak-to-peak difference between the dominant and the suppressed polarization modes of 25 dB even at substrate temperatures up to 80° C. Small-signal modulation characteristics of grating VCSELs are presented. The modulation bandwidth exceeds the required 5 GHz at a bias current of only 0.9 mA above threshold at room temperature.

1. Introduction

Owing to their low power consumption, high modulation bandwidth, and favorable beam characteristics, VCSELs are compelling light sources for miniature atomic clocks [1]. Similar to the use in tunable laser absorption spectroscopy for regular gas sensing, they must feature strictly polarization-stable single-mode emission. Additionally, they must provide narrow linewidth emission at a center wavelength of about 894.59 nm and be well suited for harmonic modulation at about 4.6 GHz in order to employ the coherent population trapping effect at the cesium D1 line [2].

Polarization stability of VCSELs is most conveniently achieved with an integrated linear semiconductor surface grating [3]. A schematic drawing of a surface grating etched in the topmost layer of the upper Bragg mirror of a VCSEL is shown in Fig. 1. The grating can be integrated in a standard VCSEL structure with very little additional processing effort and thus low cost and can be designed such that there is no penalty for laser characteristics like threshold current, differential efficiency, or far-field emission profile. Insensitivity to optical feedback and external stress has also been proven. The results are documented in a series of publications which are summarized in [3, 4]. It is worth to note that the grating-based polarization control technique was commercialized very soon after its invention and is applied today in a large fraction of 850 nm wavelength VCSEL sensors in optical navigation devices like computer mice [5, 6]. Our present work on VCSELs for Cs-based miniature atomic clocks also relies on such pure semiconductor–air surface gratings [7, 8]. In particular, so-called inverted grating VCSELs have been employed [9],

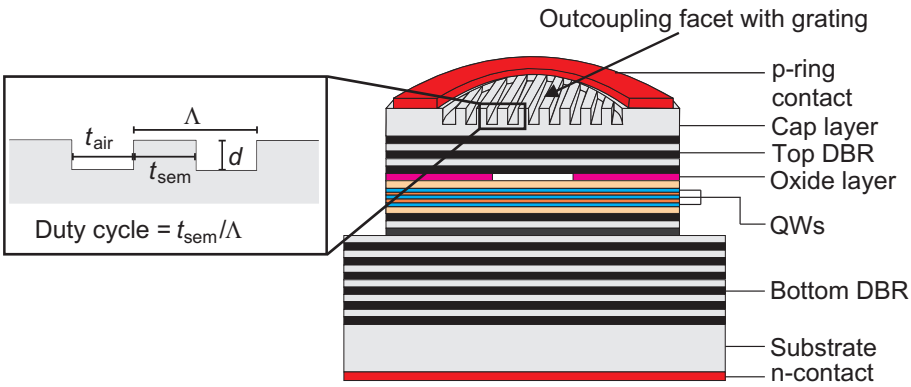

Fig. 1: Illustration of a surface grating VCSEL (right) and various grating parameters (left). Λ is the grating period, d is the grating etch depth, t_{air} and t_{sem} are the width of the grating groove and ridge, respectively.

where the grating is etched in an extra topmost GaAs quarter-wave antiphase layer. An alternative approach to full-area gratings is to etch a surface grating over a circular area of only 3 to 4 µm diameter in the center of the outcoupling facet. Such inverted grating relief VCSELs simultaneously provide favorable single-mode and single-polarization emission [10]. However, inherently higher optical losses, even of the fundamental mode, lead to larger threshold currents compared to regular inverted grating VCSELs. In this article we investigate the use of a different type of surface grating which is etched in an extra topmost half-wave GaAs in-phase layer, referred to as normal grating VCSELs. It provides lower threshold operation that is much desired for low-power atomic clock applications.

2. VCSEL Design and Fabrication

The VCSEL layers are grown on n-doped (100)-oriented GaAs substrates using solid-source molecular beam epitaxy. There is a highly n-doped GaAs contact layer above the GaAs substrate to allow n-contacting. Emission at 894.59 nm wavelength is efficiently achieved with three compressively strained 8 nm thick $In_{0.04}Ga_{0.96}As$ quantum wells (QWs) separated by 10 nm thick $Al_{0.27}Ga_{0.73}As$ barrier layers. The active region is sandwiched between two larger bandgap $Al_{0.47}Ga_{0.53}As$ cladding layers to form a one-wavelength thick inner cavity. A highly p-doped 30 nm thick AlAs layer is positioned at the node of the standing-wave pattern above the inner cavity. It is wet-thermally oxidized after mesa etching to achieve current confinement and optical index guiding. The n-type bottom and p-type top DBRs consist of 38.5 Si-doped and 25 C-doped $Al_{0.90}Ga_{0.10}As/Al_{0.20}Ga_{0.80}As$ layer pairs, respectively. The DBRs are graded in composition and doping concentration to minimize the free-carrier absorption and decrease the electrical resistance. The structure has an extra topmost GaAs cap layer in which the surface grating for polarization control is etched. The thickness of the cap layer is three quarter-wave (which is equivalent to one quarter-wave) or half-wave to construct inverted or normal VCSEL structures, respectively. In order to avoid diffraction losses in air, gratings with sub-wavelength periods of 0.6 µm and 50 % duty cycle are employed in both VCSEL types. The grating lines are etched along the [011] crystal axis, which,

resulting from the electro-optic effect, is one of the two preferred orthogonal polarization directions of standard GaAs VCSELs [3]. In the remaining part of this section, we discuss the optimization of the QW composition, the grating depth and its longitudinal position, as well as the p-DBR mirror thickness.

2.1 Active region

VCSELs to be incorporated in miniaturized atomic clock microsystems experience elevated temperatures of usually $T = 65$ to 80°C. Thus, for optimization of the active region, an experimental study with different indium content x in the $In_xGa_{1-x}As/Al_{0.27}Ga_{0.73}As$ QWs has been performed. A higher x reduces the bandgap energy and thus shifts the optical gain spectrum to longer wavelengths. Consequently, x changes the alignment between the cavity resonance (or emission wavelength) and the gain peak and hence the temperature at which the threshold current is minimized. The threshold currents of three VCSELs with different x but identical resonance wavelengths at room temperature are illustrated in Fig. 2 as a function of T. For constant x, the change of threshold current with temperature can be attributed mainly to the change of the material gain itself and the change of detuning between cavity resonance and gain peak, whereas the mirror reflectivities remain almost constant. One VCSEL has $x = 6\,\%$ and $N_p = 25$ top Bragg mirror pairs. It exhibits a minimum threshold at around 20°C. By reducing x to 4.5 % and 4 %, the point of minimum I_{th} is shifted to around 55°C and 75°C, respectively. The latter has a minimum I_{th} within the operating range of the atomic clocks. Therefore, QWs with 4 % In content have been employed in the VCSELs reported below. The magnitude of I_{th} depends on x, N_p, the active diameter as well as the presence or absence of a surface grating. The main concern of the experiments summarized in Fig. 2, however, was to optimize the point of minimum I_{th}.

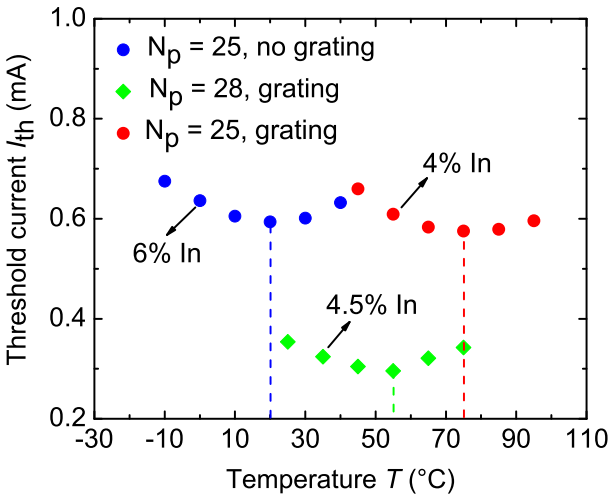

Fig. 2: Temperature dependence of the threshold current of three VCSELs with quantum wells having 6 %, 4.5 %, and 4 % indium content. The first device has 4 µm active diameter, the other two 4.5 µm. The VCSELs emit at approximately 894 nm wavelength at room temperature. They differ in the number of top mirror pairs N_p and the presence of a surface grating.

2.2 Longitudinal position of the grating

Simulations of the layer structure of 894.59 nm atomic clock VCSELs have been done using a fully vectorial, three-dimensional model based on coupled-mode theory [11, 12]. It very

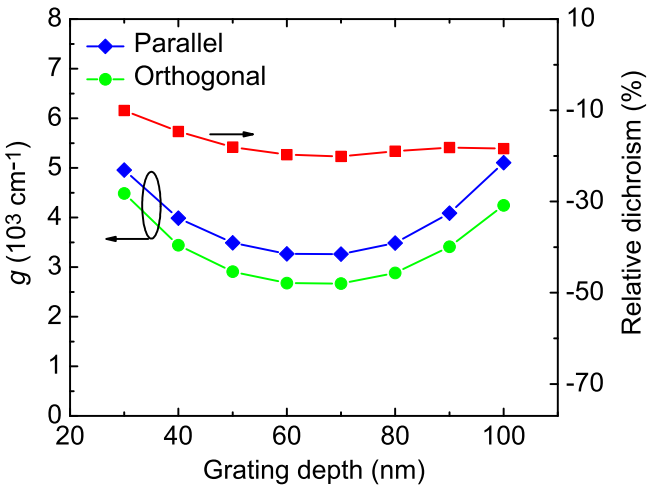

Fig. 3: Simulated material threshold gains g of the two fundamental polarization modes at $T = 20°C$ as a function of the grating depth of an inverted grating VCSEL (left axis) and the corresponding relative dichroism calculated from the threshold gains using $\mathrm{RD} = (g_{\mathrm{orth}} - g_{\mathrm{par}})/(0.5\,(g_{\mathrm{orth}} + g_{\mathrm{par}}))$ (right axis). The laser has 4 µm active diameter and $N_{\mathrm{p}} = 25$. The surface grating has 0.7 µm period and 50 % duty cycle.

well predicts the cold-cavity properties of VCSELs even with non-circular geometry [13]. Simulation results are the modal emission wavelengths, the material threshold gains of the polarization modes, as well as their field distributions. For an inverted grating VCSEL with 0.7 µm grating period and 50 % duty cycle, Fig. 3 depicts the dependence of the material threshold gains of the two fundamental transverse modes polarized parallel and orthogonal to the grating lines for grating depths d varied between 30 and 100 nm. The relative dichroisms calculated from the threshold gains are also plotted in the figure. A negative relative dichroism is observed over the whole range of grating depths, which indicates that the VCSEL emission is polarized orthogonal to the grating lines. In order to have the lowest threshold gain and hence the minimum threshold current, d should be around 70 nm, which is about one quarter of the material wavelength.

The corresponding simulation results for a normal grating VCSEL with the same active diameter, grating period, and duty cycle are depicted in Fig. 4. For grating depths below 42 nm, the threshold gain of the parallel polarization mode is larger than that of the orthogonal polarization. The situation is reverse for larger grating depths. Thus, the relative dichroism changes its sign from negative to positive at $d_{\mathrm{c}} = 42$ nm, favoring the parallel polarization for $d > d_{\mathrm{c}}$. Figure 4 shows that the material threshold gain of the selected polarization mode is minimum at around 130 nm or about half material wavelength grating depth. The minimum threshold gain is approximately 30 % of the corresponding minimum of the inverted grating VCSEL at $d = 70$ nm in Fig. 3. Reduced threshold currents of normal grating VCSELs are thus expected. The experimentally obtained I_{th} of several inverted grating and normal grating VCSELs having different active areas are displayed in Fig. 5. Both normal and inverted grating VCSELs have 0.6 µm grating period and 50 % duty cycle, however, $d = 120$ nm and 70 nm for normal and inverted grating VCSELs, respectively. Normal grating VCSELs in the lower ellipse

in Fig. 5 show an average I_{th} of about 0.2 mA, which is approximately 40 % of the I_{th} of the inverted grating VCSELs in the upper ellipse within the same range of active areas between 5 to 10 µm^2.

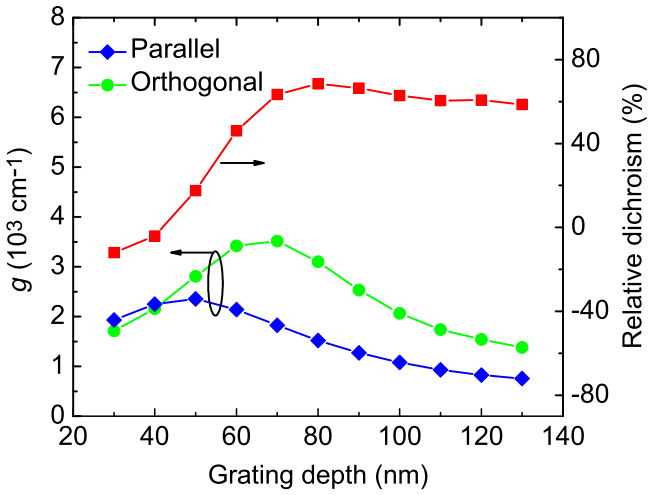

Fig. 4: Simulated material threshold gains and relative dichroism with all parameters as in Fig. 3, here for a normal grating VCSEL.

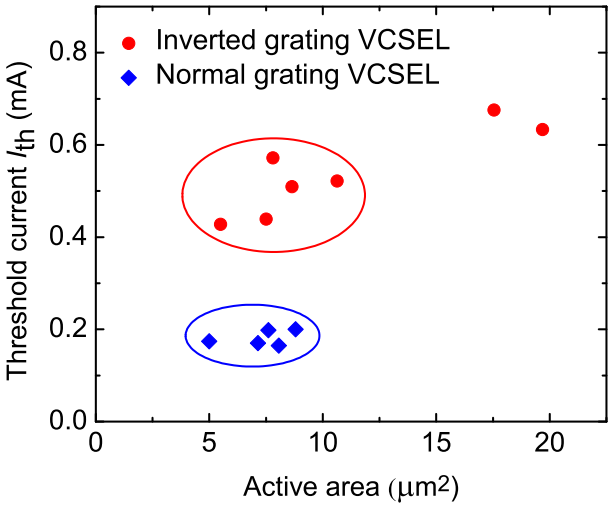

Fig. 5: Experimentally obtained threshold currents of seven inverted grating VCSELs and five normal grating VCSELs with different active areas. Inverted and normal grating devices with a similar range of active areas are grouped in two ellipses. $N_{\mathrm{p}} = 25$ and $T = 20$°C for all VCSELs.

2.3 Outcoupling mirror

A major trade-off in designing grating VCSELs are the material threshold gain and the relative dichroism achieved with different numbers of layer pairs of the outcoupling mirror. Figure 6 (top) illustrates the simulated material threshold gains of the two fundamental modes polarized parallel and orthogonal to the grating lines in dependence of the grating depth for different N_{p} of the normal grating VCSEL from Fig. 4. With increasing N_{p}, the threshold gains decrease due to the increased reflectivity of the top Bragg mirror. On the other hand, there is a lower field intensity at the surface grating (i.e., the surface grating

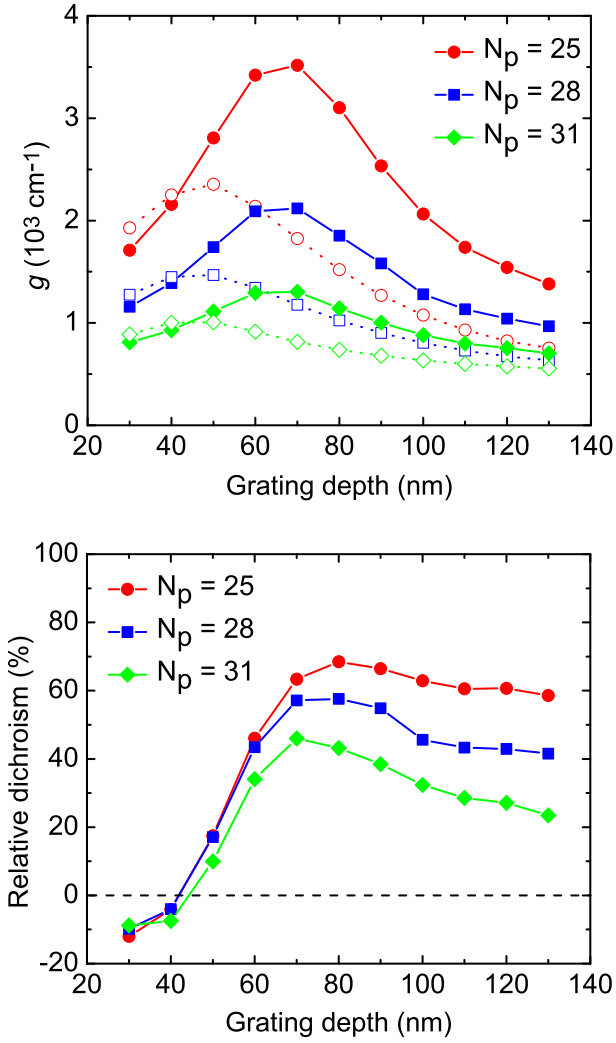

Fig. 6: Simulated material threshold gains of the two fundamental polarization modes as a function of grating depth of the normal grating VCSEL structure from Fig. 4 for different numbers of top Bragg mirror pairs N_p (top) and the corresponding relative dichroisms (bottom). The full and open symbols in the top figure represent the material threshold gains of the two fundamental modes polarized orthogonal and parallel to the grating lines, respectively.

is more decoupled from the laser cavity) and thus its polarization control effect becomes weaker. This trend is reflected in the relative dichroism which decreases with increasing N_p, as depicted in Fig. 6 (bottom). Polarization stability is a high priority for atomic clock VCSELs, to be ensured under all adverse operating conditions like high-frequency modulation or possible optical feedback in the clock microsystem. To be on the very safe side, we have limited the number of top Bragg mirror pairs in this study to 25. A higher N_p might still provide sufficient polarization stability in practice, with the benefit of further reduced I_th and higher insensitivity to optical feedback. The available output power which decreases with higher N_p is not a major concern since the clock does not require more than 100 µW. At this point, it is not possible to identify a strict upper limit for N_p.

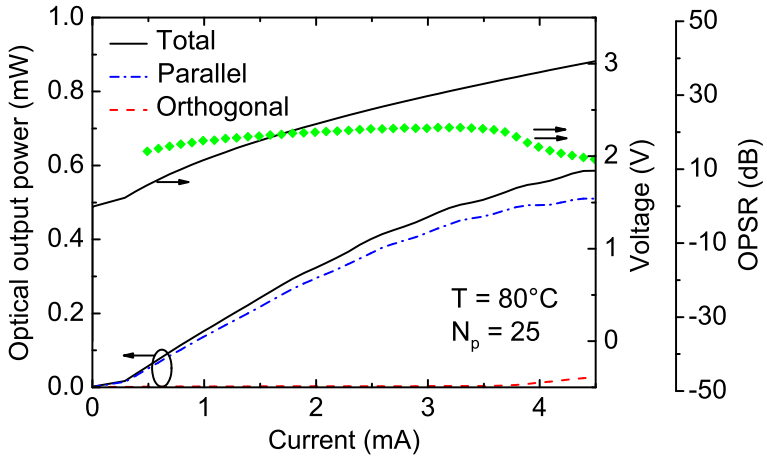

Fig. 7: Polarization-resolved operation characteristics of a normal grating VCSEL with 3 µm active diameter at 80°C substrate temperature. The grating has 0.6 µm period and 120 nm depth.

3. Experimental Results

3.1 Static characteristics

As mentioned earlier, VCSELs in Cs-based atomic clocks are exposed to temperatures T of typically 80°C. Therefore we have chosen this temperature for VCSEL characterization in the present section. Figure 7 depicts the polarization-resolved light–current–voltage (PR-LIV) characteristics of a normal grating VCSEL with an active diameter of 3 µm, a grating period of 0.6 µm and a grating depth of 120 nm. The optical powers of the two polarization modes are measured behind a Glan–Thompson polarizer by orienting its transmission direction parallel and orthogonal to the grating lines. The corresponding powers are denoted as P_{par} and P_{orth}. They are indicated in the figure by dash-dotted and dashed lines, respectively. The losses of the polarizer are responsible for the total power in Fig. 7 being larger than $P_{\mathrm{par}} + P_{\mathrm{orth}}$. The orthogonal polarization suppression ratio (OPSR) is calculated from the ratio of the two powers as $\mathrm{OPSR} = 10\log(P_{\mathrm{par}}/P_{\mathrm{orth}})$ and is displayed in the figure with green symbols. The VCSEL remains polarization-stable from its threshold current of approximately 0.2 mA up to thermal roll-over with an average OPSR of 19 dB and a peak value of 21 dB. The average OPSR is calculated from the data for currents in steps of 0.1 mA and output powers corresponding to 10 . . . 100 % of the maximum. Figure 8 shows the polarization-resolved high-temperature spectra. The target wavelength of 894.59 nm is reached at a bias current $I = 1.8$ mA with a side-mode suppression ratio (SMSR) of 42 dB. The peak-to-peak difference between the dominant and the suppressed polarization modes is about 25 dB. Both the SMSR and the peak-to-peak difference between the dominant and suppressed polarization modes far exceed the target values of 20 dB. The dominant polarizations of the normal grating VCSELs are always found to be parallel to the grating lines, which is consistent with the simulation results in Fig. 4 for about 120 nm grating depth. Figure 9 illustrates experimentally obtained average OPSRs of several normal and inverted grating VCSELs having 0.6 µm grating period. The normal and inverted grating VCSELs have 120 nm and 70 nm grat-

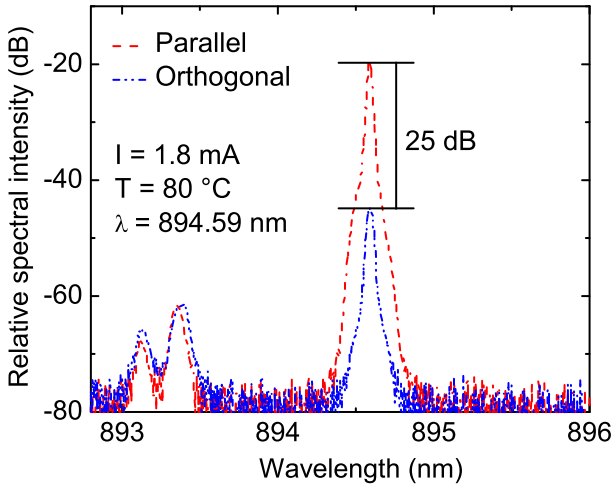

Fig. 8: Polarization-resolved spectra of the grating VCSEL from Fig. 7 at $I = 1.8\,\mathrm{mA}$ and $T = 80°\mathrm{C}$.

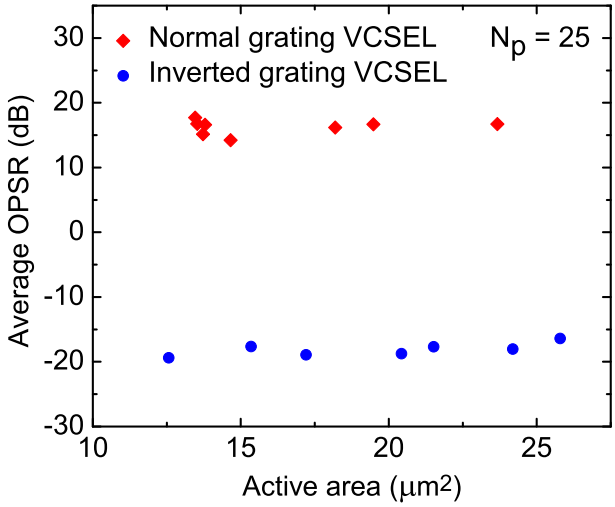

Fig. 9: Experimentally obtained average OPSRs of several normal and inverted grating VCSELs with different active areas at 80°C substrate temperature. The gratings have 0.6 µm period and 120 nm (70 nm) depth for normal (inverted) grating VCSELs.

ing depth, respectively. Positive OPSRs indicate the dominant polarization modes of the normal VCSELs to be parallel to the grating lines. In contrast, the dominant polarization of the inverted grating VCSELs is orthogonal to the grating, thus OPSR $< 0\,\mathrm{dB}$. It is worth noting that VCSELs in Fig. 9 with active areas larger than about $20\,\mu\mathrm{m}^2$ tend to be transverse multimode at higher currents. As is well known [3, 4], surface gratings also stabilize the polarization of higher-order modes.

3.2 Emission far-fields

The effect of the surface grating on the beam properties of normal grating VCSELs is investigated by measuring the emission far-fields. Figure 10 shows the far-fields parallel and

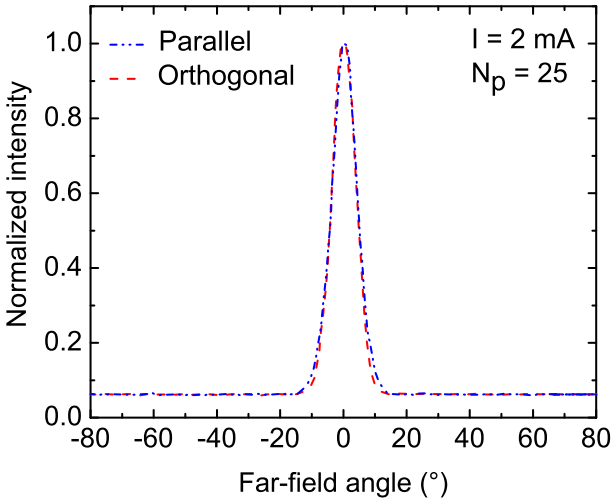

Fig. 10: Emission far-fields of a normal grating VCSEL with an active diameter of 4.8 µm, measured at $T = 20°C$. The almost overlapping dash-dotted and dashed lines indicate the normalized optical intensity parallel and orthogonal to the grating lines, respectively.

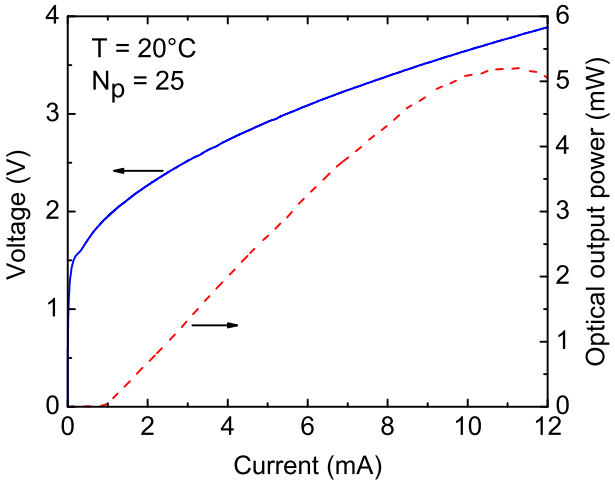

Fig. 11: LIV characteristics of a grating VCSEL with 5.3 µm active diameter.

orthogonal to the grating lines of a normal grating VCSEL with 4.8 µm active diameter at $I = 2$ mA and $T = 20°C$. The grating depth is 120 nm and the period is 0.6 µm. The absence of side-lobes in the emission far-fields proves that VCSELs with sub-emission-wavelength grating periods do not suffer from diffraction losses in air. Almost identical far-field patterns along the parallel and orthogonal directions indicate a circular beam profile. The Gaussian-like shape reflects the single-mode emission of the VCSEL at the given current.

3.3 Small-signal modulation response

Cs-based miniature atomic clocks require VCSELs with modulation bandwidths exceeding 5 GHz. The dynamic behavior of normal grating VCSELs is described in this section. The small-signal modulation responses are measured using a setup similar to the one described in [7]. LIV characteristics of a VCSEL with 5.3 µm active diameter are presented in Fig. 11 at $T = 20°C$. Figure 12 displays the small-signal modulation curves of the VCSEL at different bias currents. The threshold current is 0.90 mA. As usual it is observed that at higher bias currents, both the resonance frequency and the damping increase.

The maximum 3 dB bandwidth of 11.8 GHz is obtained at $I = 7.0$ mA. A bandwidth of 5.6 GHz, already exceeding the target value of 5 GHz, is obtained at $I = 1.8$ mA, i.e., only 0.9 mA above threshold.

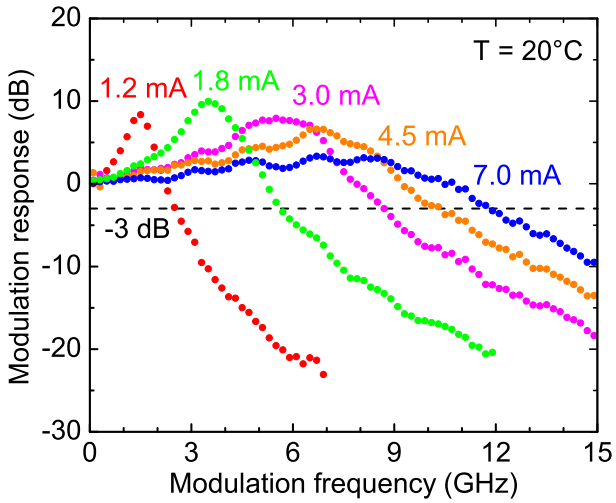

Fig. 12: Small-signal modulation response curves of the device from Fig. 11 at different bias currents and $T = 20$°C.

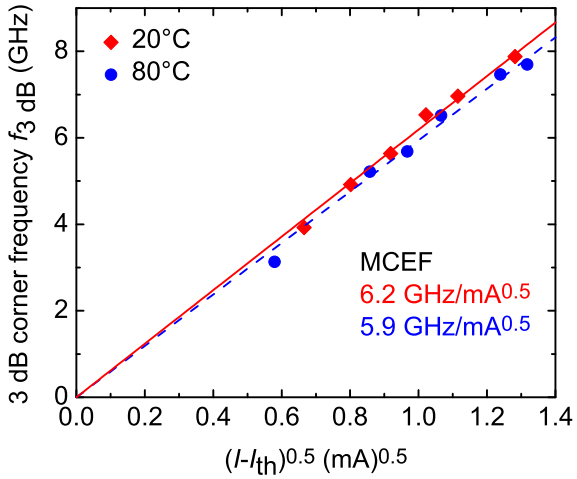

Fig. 13: 3 dB corner frequencies as a function of $\sqrt{I - I_{\mathrm{th}}}$ for the grating VCSEL from Figs. 11 and 12 at $T = 20$°C (solid) and 80°C (dashed). The MCEFs are determined from the slopes of the linear fits.

In order to determine the modualtion current efficiency factor (MCEF) defined as MCEF $= f_{3\,\mathrm{dB}}/\sqrt{I - I_{\mathrm{th}}}$, 3 dB corner frequencies $f_{3\,\mathrm{dB}}$ of the VCSEL are extracted from the small-signal modulation responses and plotted against $\sqrt{I - I_{\mathrm{th}}}$ in Fig. 13. Equivalent measurements of modulation responses and LIV characteristics of the same VCSEL were also performed at 80°C and the $f_{3\,\mathrm{dB}}$ are included in Fig. 13. The MCEFs are determined from linear fits. Values of 6.2 and 5.9 GHz/$\sqrt{\mathrm{mA}}$ are obtained at 20 and 80°C, respectively. The smaller MCEF at higher temperature is likely due to reductions of the current injection efficiency and the differential gain coefficient.

4. Conclusion

By simulations as well as experiments, we have shown that normal grating VCSELs have inherently lower threshold currents than equivalent inverted grating devices. Such low threshold, single-mode, and polarization-stable VCSELs emitting at 894.59 nm wavelength have been fabricated for use in Cs-based atomic clocks. The dynamic laser properties have been reported. The required modulation bandwidth of 5 GHz is reached close above threshold. These optimized VCSELs are very well suited for use in the next generation of European miniature atomic clock demonstrators.

Acknowledgment

The authors thank Y. Men for performing the electron-beam lithography steps and R. Rösch for reactive-ion etching. This work was funded in parts by the European Commission within its seventh framework programme (project MAC-TFC, grant agreement number 224132, http://www.mac-tfc.eu, last visited Feb. 2013).

References

[1] S. Knappe, V. Shah, P.D.D. Schwindt, L. Hollberg, J. Kitching, L.A. Liew, and J. Moreland, "A microfabricated atomic clock", *Appl. Phys. Lett.*, vol. 85, no. 9, pp. 1460–1462, 2004.

[2] J. Vanier, M.W. Levine, S. Kendig, D. Janssen, C. Everson, and M.J. Delaney, "Practical realization of a passive coherent population trapping frequency standard", *IEEE Transactions on Instrumentation and Measurement*, vol. 54, no. 6, pp. 2531–2539, 2005.

[3] J.M. Ostermann and R. Michalzik, "Polarization Control of VCSELs", Chap. 5 in *VCSELs — Fundamentals, Technology and Applications of Vertical-Cavity Surface-Emitting Lasers*, R. Michalzik (Ed.), Springer Series in Optical Sciences, vol. 166, pp. 147–179. Berlin: Springer-Verlag, 2013.

[4] R. Michalzik, J.M. Ostermann, and P. Debernardi, "Polarization-stable monolithic VCSELs", in *Vertical-Cavity Surface-Emitting Lasers XII*, C. Lei, J.K. Guenter (Eds.), Proc. SPIE 6908, pp. 69080A-1–16, 2008.

[5] M. Grabherr, R. King, R. Jäger, D. Wiedenmann, P. Gerlach, D. Duckeck, and C. Wimmer, "Volume production of polarization-controlled single-mode VCSELs", in *Vertical-Cavity Surface-Emitting Lasers XII*, C. Lei, J.K. Guenter (Eds.), Proc. SPIE 6908, pp. 690803-1–9, 2008.

[6] M. Grabherr, H. Moench, and A. Pruijmboom, "VCSELs for Optical Mice and Sensing", Chap. 18 in *VCSELs — Fundamentals, Technology and Applications of Vertical-Cavity Surface-Emitting Lasers*, R. Michalzik (Ed.), Springer Series in Optical Sciences, vol. 166, pp. 521–538. Berlin: Springer-Verlag, 2013.

[7] A. Al-Samaneh, S. Renz, A. Strodl, W. Schwarz, D. Wahl, and R. Michalzik, "Polarization-stable single-mode VCSELs for Cs-based MEMS atomic clock applications", in *Semiconductor Lasers and Laser Dynamics IV*, K. Panajotov, M. Sciamanna, A.A. Valle, R. Michalzik (Eds.), Proc. SPIE 7720, pp. 772006-1–14, 2010.

[8] A. Al-Samaneh, M.B. Sanayeh, S. Renz, D. Wahl, and R. Michalzik, "Polarization control and dynamic properties of VCSELs for MEMS atomic clock applications", *IEEE Photon. Technol. Lett.*, vol. 23, no. 15, pp. 1049–1051, 2011.

[9] J.M. Ostermann, P. Debernardi, and R. Michalzik, "Optimized integrated surface grating design for polarization-stable VCSELs", *IEEE J. Quantum Electron.*, vol. 42, no. 7, pp. 690–698, 2006.

[10] A. Al-Samaneh, M. Bou Sanayeh, M.J. Miah, W. Schwarz, D. Wahl, A. Kern, and R. Michalzik, "Polarization-stable vertical-cavity surface-emitting lasers with inverted grating relief for use in microscale atomic clocks", *Appl. Phys. Lett.*, vol. 101, pp. 171104-1–4, 2012.

[11] G.P. Bava, P. Debernardi, and L. Fratta, "Three-dimensional model for vectorial fields in vertical-cavity surface-emitting lasers", *Phys. Rev. A*, vol. 63, no. 2, pp. 023816-1–13, 2001.

[12] P. Debernardi and G.P. Bava, "Coupled mode theory: a powerful tool for analyzing complex VCSELs and designing advanced device features", *IEEE J. Select. Topics Quantum Electron.*, vol. 9, no. 3, pp. 905–917, 2003.

[13] P. Debernardi, "Three-Dimensional Modeling of VCSELs", Chap. 3 in *VCSELs — Fundamentals, Technology and Applications of Vertical-Cavity Surface-Emitting Lasers*, R. Michalzik (Ed.), Springer Series in Optical Sciences, vol. 166, pp. 77–117. Berlin: Springer-Verlag, 2013.